Coherent diffuse neutron scattering from the anion-excess fluorite $(Sr,Y)Cl_{2.03}$

1992 J. Phys.: Condens. Matter 4 1433

(http://iopscience.iop.org/0953-8984/4/6/008)

J. Phys.: Condens. Matter 4 (1992) 1433–1446. Printed in the UK

Coherent diffuse neutron scattering from the anion-excess fluorite $(Sr,Y)Cl_{2.03}$

J P Goff†‡, M T Hutchings†, S Hull§, B Fåk¶ and W Hayes‡

† NDT Department, AEA Technology, Harwell Laboratory, Didcot, Oxon, OX11 ORA, UK

‡ Clarendon Laboratory, Parks Road, Oxford, OX1 3PU, UK

§ ISIS Science Division, Rutherford Appleton Laboratory, Chilton, Oxon, OX11 OQX, UK

¶ Institut Laue–Langevin, BP 156X, Grenoble 38042, France

Received 17 October 1991

Abstract. The anion-excess fluorite $(Sr,Y)Cl_{2.03}$ has been studied by coherent diffuse neutron scattering techniques. At ambient temperature the disorder is found to be static within instrumental resolution. The parameters of defect cluster models have been fitted directly to the data. Excess chlorine ions are found to aggregate into cuboctahedral clusters whose ionic coordinates agree with those calculated from a simple hard sphere model. At elevated temperatures the scattering exhibits quasi-elastic energy broadening, indicating the dynamic nature of the disorder. Data obtained at 1050 K show that the cuboctahedral clusters have broken up, the scattering being reminiscent of that obtained from pure fluorites in the fast-ion phase. It is possible to account for the high temperature scattering in terms of 'snapshot' models of the diffusing anions and their associated relaxation fields.

1. Introduction

Strontium chloride, which has the fluorite structure (space group $Fm3m$), exhibits a marked Schottky-type specific heat anomaly at a temperature $T_c \sim 1000$ K, well below its melting point $T_m = 1146$ K. In the vicinity of T_c the ionic conductivity rises rapidly, approaching the value of the molten salt [1, 2]. This behaviour is associated with a diffuse transition to a state of relatively high, dynamic, anion disorder. In the fast-ion phase thermally generated Frenkel interstitials form short-lived, fluctuating clusters with anion vacancies and relaxed anions [3, 4]. Anions are found to hop predominantly between nearest-neighbour regular lattice sites [5, 6].

Doping with trivalent cations is found to increase the low temperature ionic conductivity and to substantially depress the transition temperature T_c [7]. In the heavily doped anion-excess fluorite $(Pb,U)F_{2+\delta}$ considerable broadening and suppression of the peak value of the specific heat anomaly has been reported [8]. Thus, below T_c the result of doping is a decrease in activation energy for both defect formation and mobility. At temperatures well above T_c the conductivity is found to level off at the value found for the undoped compound.

The fluorite crystal structure can be viewed as a simple cubic array of anions with alternate cube centres occupied by cations. Trivalent dopant cations are found to

0953-8984/92/061433+14$04.50

substitute onto regular cation sites. High dopant concentrations are possible because the relatively open structure allows charge compensating anions to be incorporated into the lattice. At low dopant concentrations, less than 1 mol%, charge compensating interstitials occupy empty cube centre sites [2]. However at higher concentrations the results of neutron diffraction studies suggest that there is no significant occupation of these sites. In $UO_{2+\delta}$ [9] and $(Ca,Y)F_{2+\delta}$ [10, 11] two types of interstitial site are found displaced in the $\langle 110 \rangle$ and $\langle 111 \rangle$ directions from the cube centres, whereas in $(Sr,Pr)Cl_{2+\delta}$ [12] and $(Ba,Pr)Cl_{2+\delta}$ [13] it is suggested that only the $\langle 110 \rangle$ sites are occupied. Defect cluster models have been developed to explain the relative occupation of such sites.

Deviations from the perfect lattice arrangement give rise to the coherent diffuse neutron scattering observed between the sharp Bragg reflections. Since the diffuse scattering derives from the spatial correlations between defective species within clusters and the regular ions it allows the defect structure to be studied more directly than by the more established technique, Bragg diffraction, which gives the time-averaged occupation of the unit cell. The analysis of diffraction data on fluorites has been reported to give rise to a possible methodological error [13], arising from overlap of the nuclear density distributions of $\langle 110 \rangle$ interstitials at $\langle 111 \rangle$ sites. This could be a problem if the temperature factor of defective anions is large at low temperature [14], and the temperature factor may lead to ambiguity in the interpretation of high temperature data. Furthermore, apart from data close to Bragg reflections, phonon contributions can be separated from diffuse scattering by means of energy analysis. This is clearly not possible for diffraction, where a correction must be made for thermal diffuse scattering. Also the ability to resolve the spectral lineshape probes the dynamic nature of the disorder, allowing the study of diffusional processes within the system.

In this paper we report studies of the coherent diffuse neutron scattering intensity, $S^D(Q)$, from single crystal samples of $(Sr,Y)Cl_{2.03}$ both at room temperature and at $T = 1050$ K, well above the transition to the fast-ion phase. By fitting the parameters of a number of trial defect clusters to the room temperature data we are able to conclusively identify the best model. In the fast-ion phase, where quasi-elastic energy broadening occurs, $S^D(Q)$ is interpreted in terms of dynamic cluster models. In a forthcoming paper we will consider how the spectral lineshape of both the coherent and incoherent scattering relates to the diffusional processes in this system. A brief report of this work has already been presented [15].

2. Theory

2.1. Neutron scattering

The incident and final neutron wavevectors (energies) are denoted k_i and k_f (E_i and E_f) respectively. $E_i = \hbar^2 k_i^2 / 2m$, where m is the neutron mass. The scattering vector is defined by $Q = k_i - k_f$ and the energy transfer by $\hbar\omega = E_i - E_f$. It is possible to express the differential cross section for neutron scattering from an assembly of one species of ion in a form which distinguishes between coherent and incoherent scattering [16, 17]:

$$\frac{d^2\sigma}{d\Omega\, dE_f} = \frac{\sigma_{coh}}{4\pi}\frac{k_f}{k_i} NS(Q,\omega) + \frac{\sigma_{incoh}}{4\pi}\frac{k_f}{k_i} NS_i(Q,\omega) \qquad (1)$$

where $S(Q,\omega)$ is the Van Hove total scattering function [18], $S_i(Q,\omega)$ is the incoherent scattering function, and N is the number of particles in the system. These scattering functions are related by double Fourier transform to the time-dependent total pair correlation function $G(r,t)$ and to the time-dependent self-correlation function $G_s(r,t)$ respectively. Intermediate functions, $I(Q,t)$, may also be defined, whose relationships are

$$S(Q,\omega) = \frac{1}{2\pi\hbar}\int G(r,t)e^{i(Q\cdot r-\omega t)}\,dr\,dt \tag{2}$$

$$G(r,t) = \frac{1}{(2\pi)^3}\int I(Q,t)e^{-iQ\cdot r}\,dQ \tag{3}$$

$$I(Q,t) = \frac{1}{N}\sum_{jj'}\langle e^{-iQ\cdot R_j(0)}e^{iQ\cdot R_{j'}(t)}\rangle. \tag{4}$$

The coherent scattering thus gives direct information on $G(r,t)$, which gives the spatial and temporal correlations between nuclei. In the classical limit $G(r,t)dr$ gives the probability that, given a nucleus at the origin at $t = 0$, any nucleus will be found within volume dr at r and at time t.

If one integrates the coherent scattering function $S(Q,\omega)$ over all energy transfers $\hbar\omega$ at constant Q one obtains the static structure factor [16]

$$\frac{d\sigma^{qs}_{coh}}{d\Omega} = \frac{\sigma_{coh}}{4\pi}N\hbar\int S(Q,\omega)\,d\omega = \frac{\sigma_{coh}}{4\pi}NS(Q). \tag{5}$$

$$S(Q) = \hbar\int S(Q,\omega)\,d\omega = I(Q,0) = \int G(r,0)e^{iQ\cdot r}\,dr = 1 + \int g(r)e^{iQ\cdot r}\,dr \tag{6}$$

where $G(r,0) = \delta(r) + g(r)$, and $g(r)$ is the static pair distribution function giving the average nuclear density at r with respect to any nucleus at the origin. From equation (4) it is seen that $I(Q,0)$ describes the instantaneous correlations between the nuclei, and so $S(Q)$ gives a 'snapshot' picture of their arrangement. In contrast, the purely elastic coherent cross section giving the scattering at $\omega = 0$ is related to $I(Q,\infty)$, the Fourier transform of $G(r,\infty)$, and gives a time-averaged picture of the arrangement of nuclei. In the case of a regular lattice of nuclei this is obtained from the Bragg peak intensities. Using the periodicity of the lattice one finds that, in general, the coherent scattering function can be written as

$$S(Q,\omega) = S^B(Q,0) + S^P(Q,\omega) + S^D(Q,\omega) \tag{7}$$

where the first term gives the elastic Bragg scattering, the second the phonon scattering and the third the diffuse scattering. By making measurements away from Bragg points and by means of energy analysis we restrict the integration in equation (6) to just the diffuse component, where the integral over $S^D(Q,\omega)$ gives $S^D(Q)$.

In practice it is not possible to Fourier transform the coherent scattering data to yield $G(r,t)$. Instead, the data are usually interpreted in terms of a model of the disordered ions at assumed positions $R_{j'}(0)$ in the expression for $I(Q,0)$ in equation (4). The summation over ions may be converted to one over sites by defining the probability of occupation of each site in the crystal. For diffuse scattering ($Q \neq \tau$)

we can calculate the coherent cross section from the occupation of sites relative to the ideal lattice. Thus, a defect cluster model enables us to calculate the structure factor, $F_i(Q)$, from

$$F_i(Q) = \sum_j (p_j - c_j)\bar{b}_j e^{-W_j(Q)} e^{-iQ\cdot r_j} \tag{8}$$

where the sum is over sites j, at r_j relative to an origin, occupied by ions of scattering length b_j, Debye–Waller factor W_j, with probability p_j (0 or 1). c_j is unity when site j coincides with a regular lattice site and zero elsewhere. If there is no correlation between the positions of the clusters the scattering from each cluster is added incoherently. All possible orientations and configurations of the cluster may be expected with equal probability. The coherent diffuse scattering per defective anion is given by

$$S^D(Q) = \frac{1}{N_i N_o} \sum_i^{N_o} F_i(Q) F_i^*(Q) \tag{9}$$

where N_i is the number of defective anions in the cluster and N_o is the number of possible orientations of the cluster. The experimentally determined coherent diffuse scattering can be placed on an absolute scale by reference to the intensity of transverse acoustic phonon excitations [4]. A comparison of the calculated intensity with the experimental intensity normalized as the scattering per unit cell yields the number of defective anions per unit cell, and hence δ, the excess Cl^- ion concentration, in $(Sr,Y)Cl_{2+\delta}$. Since the concentration of dopant ions can also be found by other techniques, this provides an independent test of the analysis procedure.

2.2. *Cluster models*

The cuboctahedral cluster, shown in figure 1(*a*), is related to those found in the fluorite superstructures of β-U_4O_9 [19, 20], $Ca_{14}Y_5F_{43}$ [21] and Ca_2YbF_7 [22]. To visualize this model it is useful to consider an empty cube site surrounded by an octahedron of cations enclosed by six cubes of anions; these share edges to give a unit of composition M_6X_{32}. Each cube can be converted to a square antiprism of anions by rotation of one of its faces by 45°. The cuboctahedral cluster comprises six such antiprisms of anions sharing corners to give a cluster of composition M_6X_{36}, i.e. with four extra anions per cluster.

Smaller defect clusters have been proposed for other anion-excess fluorite systems. Isolated square antiprisms, which are fragments of cuboctahedral units, have been suggested for $(Ca,Y)F_{2+\delta}$ [23]. 'Willis' clusters are found to account for the diffuse neutron scattering from $(Ba,La)F_{2+\delta}$ [24] and $UO_{2.13}$ at elevated temperature [25]. The simplest cluster of the 'Willis' type is the 2:1:2 cluster, where the notation—vacancies: 'true' interstitials: relaxed anions—is used, see figure 1(*b*). The 'true' interstitial anion, at a site displaced by $(y, \bar{y}, 0)$ from the centre of the cube edge, causes the two nearest-neighbour anions to relax by (x, x, x) towards empty cube centres. The 2:2:2 'Willis' cluster is similar, but with an additional 'true' interstitial occupying the symmetrical site and displaced by $(\bar{y}, y, 0)$. The relaxing anions may in turn cause the six next-nearest-neighbour anions to relax outwards by (z, z, z) towards empty cube centres, giving 8:1:8 and 8:2:8 clusters.

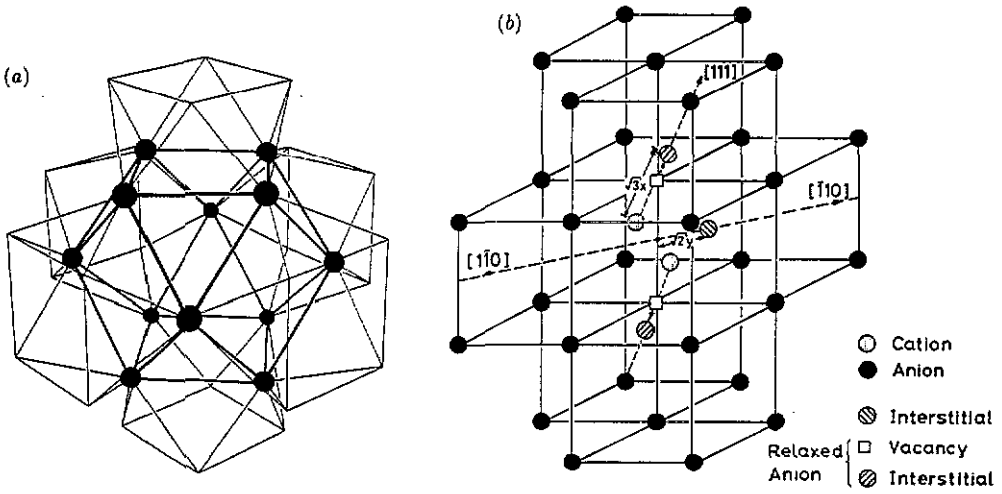

Figure 1. Defect cluster models proposed for anion-excess fluorites: (*a*) cuboctahedral model, where an empty cube centre is surrounded by twelve interstitial anions in ⟨110⟩ directions rather than the usual eight regular anions at the cube vertices; (*b*) 2:1:2 cluster, where an interstitial anion displaced in a ⟨110⟩ direction from a cube edge centre causes relaxation of the two nearest-nearest-neighbour anions in ⟨111⟩ directions towards empty cube centres.

3. Experimental procedure

Single crystal samples of $(Sr,Y)Cl_{2.03} \simeq 1$–2 cm^3 in volume were grown from the melt by the Czochralski pulling technique at the Clarendon Laboratory by R C C Ward. The concentration of dopant, measured by atomic absorption spectrometry, was found to vary over the sample in the range 2.5–3.2 mol%. Cylindrical boules were aligned and mounted inside cans with the [1$\bar{1}$0] crystallographic axis vertical. One sample, sealed in a dry atmosphere inside an aluminium can, was examined at ambient temperature on the triple axis spectrometer, PLUTO reactor, Harwell. Experiments were performed at elevated temperature using the triple axis spectrometer IN12 at the Institut Laue–Langevin, Grenoble. For these experiments the sample was encapsulated under vacuum inside a molybdenum tube, and mounted inside a specially designed furnace for neutron scattering. A summary of experiments performed, together with the instrumental set-up used, is provided in table 1.

Table 1. Summary of experiments and instrumental set-ups used. The collimator angles refer to those before the monochromator, sample, analyser and detector respectively. The resolution given is the FWHM of the vanadium scan.

Expt	Date	Instrument	k_i (Å^{-1})	Collimation	Resolution (meV)
I	Aug.88	PTA Harwell	4.05	75′ 20′ 30′ 60′	3.50
II	Jan.91	IN12 ILL	2.00	26′ 30′ 30′ 60′	0.31
III	Jan.91	IN12 ILL	2.10	25′ 30′ 120′ 60′	0.54
IV	Jan.91	IN12 ILL	1.50	34′ 30′ 30′ 60′	0.12

The resolution function of triple axis spectrometers has been discussed elsewhere [26]. The variation of the cross section with Q is not large over the resolution aper-

ture in Q for the broad peaks reported here. However, the overall instrumental energy resolution, which is determined from an energy scan of the incoherent scattering from vanadium, must be carefully adjusted. In order to detect quasi-elastic energy-broadening high energy resolution is required. This is achieved with narrow collimation and the low k_i available on IN12, which is situated on a high-flux cold neutron source. In order to measure $S^D(Q)$ we require the instrumental energy resolution to be much broader than the quasi-elastic peak so that the instrument measures the integrated intensity. However, away from the Bragg reflections the instrumental resolution window centred on zero energy transfer must be sufficiently narrow to exclude phonon excitations. The relatively poor collimation and high k_i obtained from the thermal source in the PLUTO reactor give suitable resolution. It is noted that, although a high k_i is necessary to extend the data acquisition to high Q, the accompanying increase in resolution width worsens phonon contamination near Bragg points. Thus, as well as excluding the scattering at Bragg points it is necessary to discard data from a region within approximately 0.1 reciprocal lattice units (rlu) of strong reflections. It is also necessary to remove from the analysis the scattering arising from powder diffraction from the sample can. Contamination of the incident beam by $\lambda/2$ was minimized by use of either a pyrolytic graphite filter for $k_i \geqslant 2.5$ Å^{-1} or a cooled beryllium filter for $k_i \leqslant 1.57$ Å^{-1}.

4. Results

4.1. $S(Q)$ at ambient temperature

The coherent diffuse scattering in the $(1\bar{1}0)$ plane at room temperature, measured in experiment I, see table 1, is presented in figure 2(*a*). In experiment IV it was found to be elastic within the instrumental energy resolution (0.12 meV). This tells us that $S^D(Q)$ is given by $S^D(Q,0)$ in experiment I and that the clusters had a minimum lifetime $\tau_{coh} \simeq 100$ ps [4]. The fact that the scattering is highly anisotropic rules out the possibility that anions are randomly distributed over the lattice on 'empty' cube centre sites. The width of the peaks in Q are consistent with the presence of small defect clusters. Since no sharper superlattice reflections are observed it is reasonable to conclude that there is no significant correlation between clusters. The scattering differs from that observed in pure fluorite compounds at high temperature [4], the peaks being more rounded and well defined.

Least-squares fits of the positional and thermal parameters of possible defect cluster models were made to the intensity at the elastic point $S^D(Q,0)$, which is related to the integrated intensity per unit cell, $S^D(Q) = N_A S^D(Q,0)$. The normalization factor, N_A, was calculated from the measured intensities of transverse acoustic phonons at $Q = (2,2,0.06)$ and $(2,2,0.1)$ [4]. The quantity minimized, χ^2, was defined by

$$\chi^2 = \frac{1}{N_d} \sum_i^{N_d} \left(\frac{S^D_{EXP}(Q_i,0) - S^D_{CAL}(Q_i)}{\Delta S^D_{EXP}(Q_i,0)} \right)^2 \tag{10}$$

where N_d is the total number of data points, the ith point taken at a scattering vector Q_i, of experimental elastic intensity $S^D_{EXP}(Q_i,0)$, experimental uncertainty $\Delta S^D_{EXP}(Q_i,0)$ and calculated intensity $S^D_{CAL}(Q_i)$.

$$S^D_{CAL}(Q) = f S^D(Q) + (A_1 - A_2 Q) \tag{11}$$

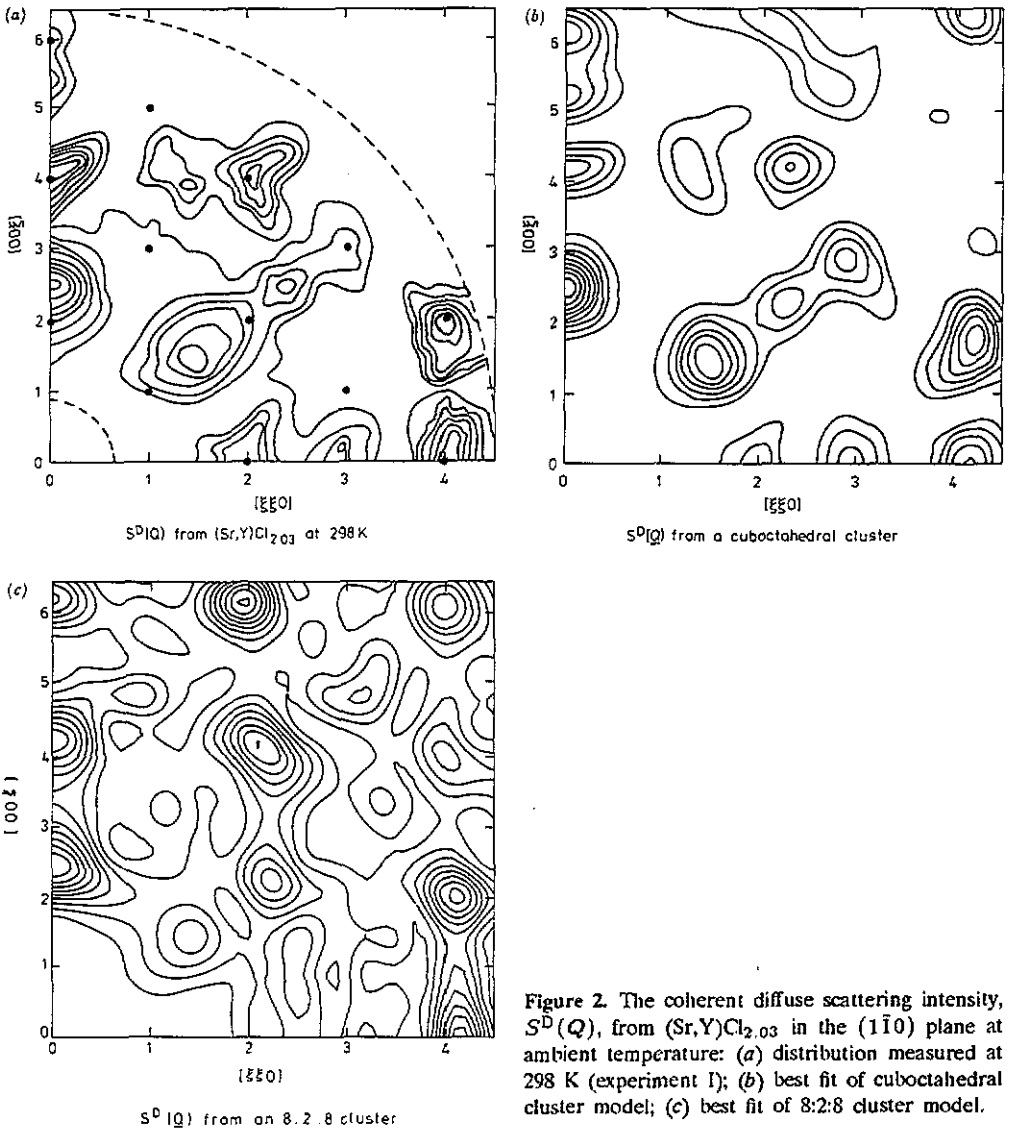

Figure 2. The coherent diffuse scattering intensity, $S^{D}(\boldsymbol{Q})$, from $(Sr,Y)Cl_{2.03}$ in the $(1\bar{1}0)$ plane at ambient temperature: (*a*) distribution measured at 298 K (experiment I); (*b*) best fit of cuboctahedral cluster model; (*c*) best fit of 8:2:8 cluster model.

where the calculated scattering per defective anion, $S^{D}(Q)$, is given by equations (8) and (9) and the scale factor f is related to δ in the formula $(Sr,Y)Cl_{2+\delta}$ by

$$\delta = \tfrac{1}{4} N_{A} f \tag{12}$$

since there are 4δ defective anions per unit cell. A plot of all the data against Q shows that the coherent peaks are superimposed upon a linearly varying background, described by parameters A_1 and A_2, which arises from the incoherent scattering from the sample and elastic scattering from the furnace and sample can. The results of the fits are summarized in table 2, which also contains the values of δ obtained using equation (12).

The Debye–Waller factor in equation (8) is calculated from the temperature factor

Table 2. Comparison of the 'goodness of fit' parameter, χ^2, and the defect concentration, δ, obtained by fitting different cluster models to the observed data at ambient temperature 298 K using the method of least squares.

Defect cluster model	χ^2	δ
Cuboctahedron	10.9	0.032(5)
Cuboctahedron and relaxation field	8.0	0.033(5)
Square antiprism	14.7	0.090(14)
2:1:2	20.0	0.053(8)
2:2:2	19.2	0.084(13)
8:1:8	16.6	0.040(6)
8:2:8	16.0	0.054(8)

of the defective anions, B, which is given by

$$W(Q) = B(Q/4\pi)^2. \tag{13}$$

Initial fits to the data had the temperature factors fixed at those reported for regular ions in $SrCl_2$ at ambient temperature [27], $B_{Cl} = 1.4$ Å^2 and $B_{Sr} = 1.2$ Å^2. Allowing separate temperature factors for each defective species to vary produced no significant improvement in the quality of the fit.

From the data in table 2 it is seen that the cuboctahedral cluster model fits the room temperature data much better than the 'Willis' type or isolated square antiprism models. The basic cuboctahedral model, comprising twelve cuboctahedral interstitial anions and the cube of eight anion vacancies, produces broad diffuse features at the positions shown in figure 2(*a*). Relaxation of nearby ions gives better agreement with the shape and relative intensities of the diffuse features. Table 3 presents the fitted parameters of a cuboctahedral cluster model with relaxation of nearby ions. The scattering in the $(1\bar{1}0)$ plane from such a model, shown in figure 2(*b*), is in good agreement with experiment. For comparison, the scattering from the best 'Willis' model, the 8:2:8, is shown in figure 2(*c*).

4.2. $S(Q)$ at elevated temperature

At temperatures below 900 K the diffuse scattering is found to be elastic within instrumental resolution. Figure 3(*a*) shows $S^D(Q,0) = S^D(Q)$ measured in experiment II, see table 1, with Q along the [001] direction, at several temperatures, as the sample was cooled down from 900 to 293 K. The broad diffuse peak moves away from the Bragg point as the temperature is decreased.

At temperatures of 900 K and above a quasi-elastic broadening of the diffuse scattering is observed in experiment IV showing that the disorder is becoming dynamic in nature. The elastic intensity, $S^D(Q,0) \sim S^D(Q)$, measured in experiment III along the [001] axis at temperatures between 900 and 1050 K is presented in figure 3(*b*). The reduction in observed intensity with temperature increase is due in part to an increase in energy broadening to greater than the instrumental resolution. The peak is seen to move out from the (002) point in much the same manner as occurs in the pure fluorites in the fast-ion phase [4].

Figure 4 shows the intensity obtained in experiment IV by scanning energy at a fixed wavevector, $Q = (0,0,2.3)$, both above and below the transition to the fast-ion phase. The low temperature data were adequately fitted by a Gaussian function of

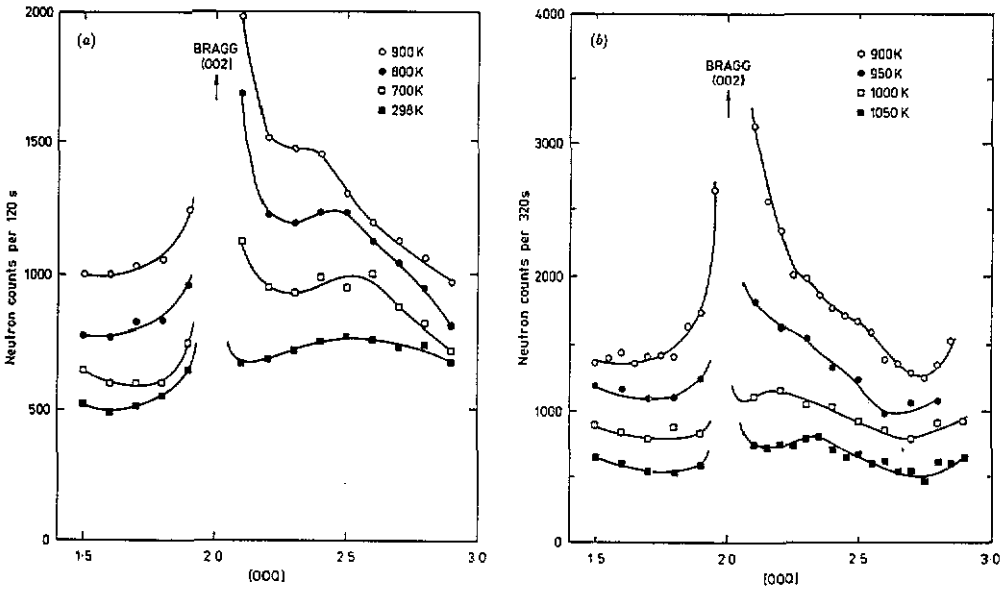

Figure 3. The elastic coherent diffuse scattering intensity, $S^{D}(Q,\omega = 0)$ along the [001] direction: (*a*) 298 to 900 K (experiment II); (*b*) 900 to 1050 K (experiment III). The scans have been offset vertically by +200 counts for each step in temperature for clarity.

instrumental resolution width, combined with a sloping background. At 1050 K the observed spectral lineshape can be fitted by the expression

$$S^{D}_{EXP}(Q,\omega) = S^{D}(Q,\omega) * R(\omega) + G(\omega) + B(\omega) \tag{14}$$

where the coherent scattering from the sample, $S^{D}(Q,\omega)$, is a Lorentzian function convolved with a resolution Gaussian function $R(\omega)$, $G(\omega)$ is the elastic scattering and resolution-limited incoherent scattering, and $B(\omega)$ is a sloping background level. (The incoherent scattering may be treated as resolution-limited in this experiment since its width is over one order of magnitude lower than the coherent width at the scattering vectors considered.) In analysing the data, corrections were made for the variation of the resolution ellipsoid with final wavevector, k_f [26]. Figure 5 presents the variation of the FWHM of the Lorentzian profile as a function of wavevector along the [001] axis. The pronounced decrease in energy width near the (002) reflection suggests that the correlations that cause the coherent diffuse scattering decay and reappear in a manner that conserves the translational symmetry of the anion sublattice [4].

In order to measure the integrated intensity $S^{D}(Q)$ at 1050 K it is necessary to perform energy scans at each wavevector. In experiment III we approximated this by measuring the elastic intensity, $S^{D}(Q,0)$, using the broadest resolution function achievable. In fact the Lorentzian width varied from very small near the anion reciprocal lattice points to roughly equal to the resolution width elsewhere, so the intensities measured were as low as 50% of the integrated value in some regions of the plane. Thus, when interpreting the grid obtained at 1050 K (figure 6(*a*)) we must only consider the qualitative features observed.

Even with these limitations it is clear that $S^{D}(Q)$ at 1050 K is markedly different from that obtained at ambient temperature. We observe an anisotropic shell of

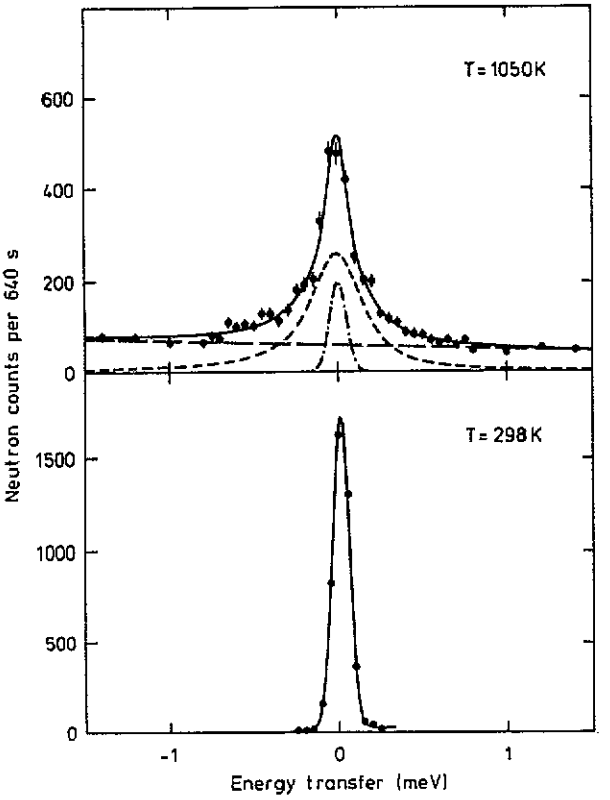

Figure 4. Scans of energy transfer at $Q = (0, 0, 2.3)$ at 298 and 1050 K (experiment IV). At ambient temperature the data are fitted by a resolution limited Gaussian plus a sloping background. Quasi-elastic broadening is observed at 1050 K. The full curve shows the fit to the data, comprising (short broken curve) a Lorentzian function convolved with the resolution function, (chain curve) a resloution-limited Gaussian function and (long broken curve) a sloping background.

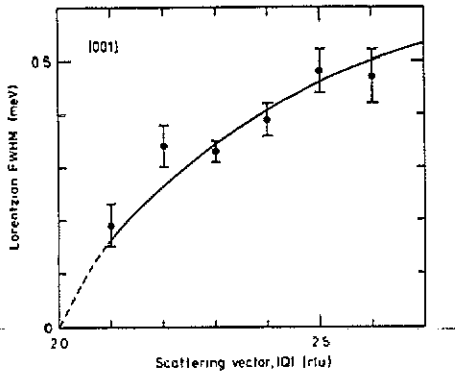

Figure 5. Variation of the FWHM of the Lorentzian profile of the coherent diffuse scattering at 1050 K with scattering vector along the [001] direction. The curve is a guide to the eye.

diffuse scattering at $Q \sim 2$ rlu, which is reminiscent of that obtained from the pure fluorites at elevated temperature [4]. It is possible to interpret the data in terms of the scattering from diffusing anions and their associated distortion field. In the 'snapshot' of the system we see an average of anions at all points in their transit for all diffusional processes in operation. However, by considering idealized defect clusters we begin to see how the peaks arise. Interstitials may temporarily form 2:1:2 clusters, and the calculated scattering from such a cluster is shown in figure 6(*b*). It is possible that such an interstitial anion could knock one of its neighbouring anions

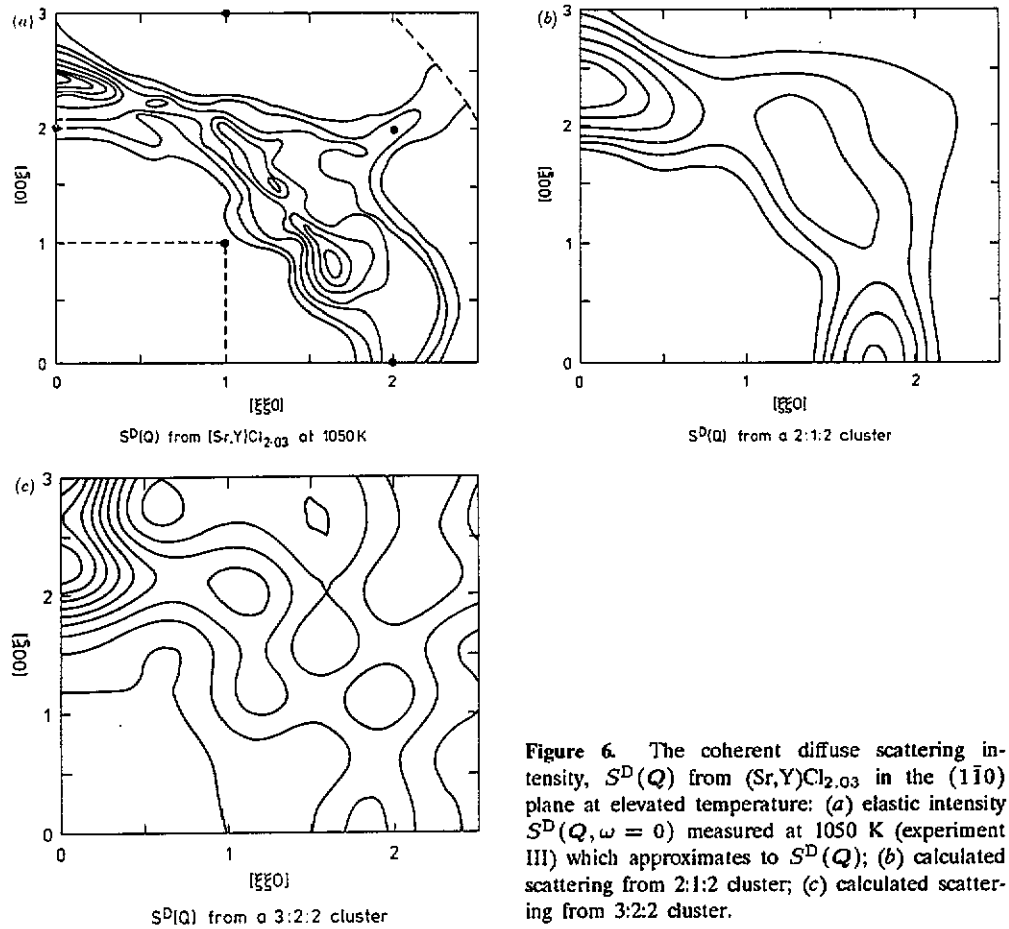

Figure 6. The coherent diffuse scattering intensity, $S^D(Q)$ from $(Sr,Y)Cl_{2.03}$ in the $(1\bar{1}0)$ plane at elevated temperature: (*a*) elastic intensity $S^D(Q, \omega = 0)$ measured at 1050 K (experiment III) which approximates to $S^D(Q)$; (*b*) calculated scattering from 2:1:2 cluster; (*c*) calculated scattering from 3:2:2 cluster.

onto a nearby $\langle yy0 \rangle$ site by the interstitialcy mechanism. An idealized snapshot of this event is the 3:2:2 cluster. This can be obtained from the 2:1:2 cluster if one of the relaxed anions is 'knocked' onto an adjacent $\langle yy0 \rangle$ site. The scattering from such a cluster is shown in figure 6(*c*). A combination of the calculated scattering from all such defect cluster models, correctly averaged, will give a good approximation to the observed $S^D(Q)$ for this disordered system.

We have estimated the fraction of anions in interstitial positions, δ', by comparing the normalized experimental intensity at $T = 1050$ K with the scattering calculated using a 2:1:2 cluster. There is an error in the value obtained due to the uncertainty of the model of the dynamic disorder. The results of neutron diffraction experiments performed on $SrCl_2$ in the fast-ion phase were used to estimate the parameters of the model, giving $y = 0.04(1)$ and $x = 0.13(1)$ [4] (see section 2.2) and $B_{Cl} = 11.0(5)$ [28]. This yields a concentration, $\delta' = 0.24(8)$, much larger than the extrinsic concentration, $\delta = 0.03$, reflecting the thermal generation of intrinsic defects at this temperature.

Table 3. Comparison of the positions of ions determined by the least-squares fit of the relaxed cuboctahedral model ($m3m$) to the ambient temperature data with the predictions of a simple hard sphere model. The coordinates are relative to an origin at the empty cube centre.

Ion	x	y	z
Positions determined in fit to diffuse scattering			
Interstitial Cl (×12)	0.357(1)	0.357(1)	0
Relaxed NN Cl (×24)	0.25	0.25	0.7648(2)
Relaxed NN Sr (×6)	0	0	0.539(2)
Relaxed NNN Sr (×8)	0.5167(1)	0.5167(1)	0.5167(1)
Positions calculated from hard sphere model			
Interstitial Cl (×12)	0.353	0.353	0
Relaxed NN Cl (×24)	0.25	0.25	0.75
Relaxed NN Sr (×6)	0	0	0.55
Relaxed NNN Sr (×8)	0.5	0.5	0.5

5. Discussion

The fitted parameters in tables 2 and 3 enable a careful assessment of the cuboctahedral model proposed for the disorder at ambient temperature. The concentration of excess anions found from the diffuse scattering is in good agreement with an independent assessment using atomic absorption spectrometry. It is possible to interpret the other fitted parameters, the positions of the defective ions, in terms of a simple hard sphere model. If we assume that the separations between the anions in the rotated faces of the square antiprisms are unaltered in the cluster, they are situated at positions $\{a_0/2\sqrt{2},\ a_0/2\sqrt{2}, 0\}$ from the centre of the cluster. Owing to the relatively tight packing of the anion sublattice in $SrCl_2$, relaxation of nearest-neighbour anions is small. However, since there are 24 of these anions per cluster, a small displacement has an appreciable effect on the diffuse scattering. If the six nearest-neighbour cations are at the centres of the square antiprisms they must relax outwards by $\{0, 0, (\frac{1}{4\sqrt{2}} - \frac{1}{8})a_0\}$. The eight next-nearest-neighbour cations are contained in distorted 'cubes' whose inner vertex is replaced by a triangle of $\{y, y, 0\}$ anions (see figure 1(a)). The three anions in these triangles are further from the cube centre than the regular anions. These cations therefore move inwards along $\langle 111 \rangle$ directions, the tight packing again limiting the displacement. Table 3 compares the ionic coordinates of the cuboctahedral model determined from fits to the room temperature diffuse scattering to the hard sphere parameters. It is seen that only the anion interstitials and nearest neighbour cations are calculated in the model. The high value of χ^2 obtained is probably due to the simplicity of the model. In the real clusters some Sr^{2+} ions are replaced by Y^{3+} ions leading to distortions from the very symmetrical ($m3m$) cluster model. However, the closeness of the fitted parameters to those predicted by these simple arguments is compelling evidence for the validity of the cuboctahedral model.

Static energy calculations have been used by a number of authors to compare the stability of various cluster models for a range of fluorites and dopant cations, and have shown that the displaced 'true' interstitials are stable with respect to the cube centre sites [29, 30]. Cuboctahedral clusters are most stable relative to smaller complexes when the dopant cation is of low ionic radius and the host lattice parameter, a_0, is

large [30]. The low Y^{3+} radius [31] together with the relatively high lattice parameter, $a_0 = 6.98$ Å, suggests that the occurrence of cuboctahedral clusters in $(Sr,Y)Cl_{2.03}$ is consistent with these theoretical considerations.

Although a previous x-ray diffraction study of $(Sr,Y)Cl_{2.05}$ has been interpreted in terms of 'Willis' clusters, the authors concede that the defect structure could be closer to the cuboctahedral structure of U_4O_9 [32]. We have shown this to be so for $(Sr,Y)Cl_{2.03}$ at ambient temperature, the principal difference being the lack of long-range ordering of the cuboctahedral units found in U_4O_9.

It is possible that the cuboctahedral clusters break up to smaller fragments, such as 8:2:8 clusters, even at temperatures below 900 K. If this is so the diffusion of anions necessary for these rearrangements is too slow to be detected by quasi-elastic broadening. However this phenomenon is also observed in $UO_{2.13}$ by coherent diffuse scattering [25]. At ambient temperature that system consists of a mixture of the UO_2 and U_4O_9 phases, and so cuboctahedral clusters are present in an ordered array. By a temperature of 858 K the long-range order is destroyed and the system comprises a single phase. Coherent diffuse neutron scattering indicates the presence of static, isolated 8:2:8 clusters.

Above 900 K dynamic disorder is observed in $(Sr,Y)Cl_{2.03}$, similar to that observed in the fast-ion phase of the pure fluorites [4]. We first notice energy broadening at 900 K, well below the temperature at which significant intrinsic disorder is detectable in pure $SrCl_2$ ($T_c = 1000$ K) [33]. The $S^D(Q)$ data at 1050 K clearly show that the cuboctahedral clusters have broken up by this temperature and that there are a large number of thermally excited defects in addition to the extrinsic defects. An interpretation in terms of 'snapshots' of diffusing ions and their associated distortion field succeeds in accounting for the major features in the observed $S^D(Q)$, and is consistent with the tendency of the energy width to display the periodicity of the anion sublattice. A similar interpretation has been reported for the $S^D(Q,\omega)$ of CaF_2 based on molecular dynamics simulations [34, 35].

6. Conclusion

The coherent diffuse neutron scattering from $(Sr,Y)Cl_{2.03}$ has been studied both at ambient temperature and within the fast-ion phase. The low temperature data have been modelled in terms of static defect clusters. We have been able to distinguish between several possible cluster models, and our results favour the cuboctahedral model. Normalization has been carried out by reference to transverse acoustic phonon excitations, from which the calculated excess of anions is in agreement with an independent determination of dopant concentration. Other fitted parameters of the model are in good agreement with a simple hard sphere model. These defect clusters are found to break up at elevated temperatures. In the fast-ion phase the scattering exhibits quasi-elastic energy broadening, demonstrating the dynamic nature of the disorder. It is possible to model the high temperature data in terms of 'snapshots' of diffusing anions and their associated relaxation field. This is consistent with the Q dependence of the energy widths. A full account of the significance of the variation of the spectral function with Q and temperature will be presented in conjunction with extensive studies of the incoherent scattering from this system in a future publication. The incoherent scattering, which is related to the mobility of individual ions, gives information on the hopping rate and geometry of chlorine ions, which is consistent with the present data.

Acknowledgments

This work was undertaken as part of the Corporate Research Programme of AEA Technology.

References

[1] Chadwick A V 1983 *Solid State Ionics* **8** 209–20
[2] Hayes W and Hutchings M T 1989 *Ionic Solids at High Temperatures* ed A M Stoneham (Singapore: World Scientific) ch 4
[3] Clausen K, Hayes W, Hutchings M T, Kjems J K, Schnabel P and Smith C 1981 *Solid State Ionics* **5** 589–92
[4] Hutchings M T, Clausen K, Dickens M H, Hayes W, Kjems J K, Schnabel P and Smith C 1984 *J. Phys. C: Solid State Phys.* **17** 3903–40
[5] Dickens M H, Hayes W, Schnabel P G, Hutchings M T, Lechner R E and Renker B 1983 *J. Phys. C: Solid State Phys.* **16** L1–6
[6] Schnabel P G, Hayes W, Hutchings M T, Lechner R E and Renker B 1983 *Radiation Effects* **75** 73–7
[7] Catlow C R A, Commins J D, Germano F A, Harley R T, Hayes W and Owen I B 1981 *J. Phys. C: Solid State Phys.* **14** 329–35
[8] Andersen N H, Clausen K and Kjems J K 1983 *Solid State Ionics* **9&10** 543–8
[9] Willis B T M 1964 *Proc. Br. Ceram. Soc.* **1** 9
[10] Cheetham A K, Fender B E F, Steele B, Taylor R I and Willis B T M 1970 *Solid State Commun.* **8** 171
[11] Cheetham A K, Fender B E F and Cooper M J 1971 *J. Phys. C: Solid State Phys.* **4** 3107
[12] Bendall P J, Catlow C R A and Fender B E F 1984 *J. Phys. C: Solid State Phys.* **17** 797
[13] Muradyan L A, Maksimov B A, Aleksandrov V B, Otroshchenko L P, Bydanov N N, Sirota M I and Simonov V I 1986 *Sov. Phys. Crystallogr.* **31** 390–2
[14] Haridasan T M, Govindarajan J, Nerenberg M A H and Jacobs P W M 1979 *J. Phys. C: Solid State Phys.* **12** 5371–9
[15] Goff J P, Clausen K, Fåk B, Hadfield R, Hayes W, Hull S and Hutchings M T 1991 *Proc. ICNS 91 (Oxford, 1991); Physica* B at press
[16] Squires G L 1978 *Introduction to the Theory of Thermal Neutron Scattering* (Cambridge: Cambridge University Press)
[17] Sköld K and Price D L 1986–7 *Methods of Experimental Physics* **23** vols A-C (New York: Academic)
[18] van Hove L 1954 *Phys. Rev.* **110** 999–1010
[19] Bevan D J M, Grey I E and Willis B T M 1986 *J. Solid State Chem.* **61** 1
[20] Willis B T M 1987 *J. Chem. Soc., Faraday Trans. 2* **83** 1073–81
[21] Bevan D J M, Greis O and Strähle J 1980 *Acta Crystallogr.* A **36** 889–90
[22] Ness S E, Bevan D J M and Rossell H J 1988 *Eur. J. Solid State Inorg. Chem.* **25** 509
[23] Laval J P and Frit B 1983 *J. Solid State Chem.* **49** 237
[24] Andersen N H, Clausen K N, Kjems J K and Schoonman J 1986 *J. Phys. C: Solid State Phys.* **19** 2377–89
[25] Goff J P, Hutchings M T, Brown K, Hayes W and Godfrin H 1990 *Mat. Res. Soc. Symp. Proc.* **166** 373–7
[26] Dorner B 1972 *Acta Crystallogr.* A **28** 319–27
[27] Dickens M H, Hayes W, Hutchings M T and Smith C 1979 *J. Phys. C: Solid State Phys.* **12** L97–102
[28] Schnabel P G 1983 *D Phil Thesis* University of Oxford p 97
[29] Corish J, Catlow C R A, Jacobs P W M and Ong S H 1982 *Phys. Rev.* B **25** 6425–38
[30] Bendall P J, Catlow C R A, Corish J and Jacobs P W M 1984 *J. Solid State Chem.* **51** 159–69
[31] Shannon R D and Prewitt C T 1969 *Acta Crystallogr.* B **25** 925–46
[32] Mason E and Eick H 1983 *J. Solid State Chem.* **47** 314–21
[33] Dickens M H, Hutchings M T, Kjems J and Lechner R E 1978 *J. Phys. C: Solid State Phys.* **11** L583–8
[34] Gillan M J 1986 *J. Phys. C: Solid State Phys.* **19** 3391–411
[35] Gillan M J 1986 *J. Phys. C: Solid State Phys.* **19** 3517–33